Numerical study of spin relaxation in a quantum wire with spin-orbit interaction

Tomoaki Kaneko, Mikito Koshino, and Tsuneya Ando
Department of Physics, Tokyo Institute of Technology, 2-12-1 Ookayama, Meguro-ku, Tokyo 152-8551, Japan
(Received 11 August 2008; revised manuscript received 4 November 2008; published 5 December 2008)

The spin-relaxation length in quantum wires with spin splitting due to the lack of the structure inversion symmetry is numerically studied using a tight-binding model. The spin-relaxation length is sensitive to the spin-split subband structure in quantum wires. When the spin splitting is smaller than the subband separations, the quantized one-dimensional subbands have a well-defined spin and the spin-relaxation length is considerably enhanced with the decrease in the width.

DOI: 10.1103/PhysRevB.78.245303 PACS number(s): 73.23.−b, 72.25.−b, 73.21.Hb

I. INTRODUCTION

Development of spintronics which utilizes the spin degree of freedom in electronics devices makes spin-related phenomena in semiconductor highly interesting.[1,2] To achieve this new electronics, long spin coherence or long relaxation length should be required. The purpose of this paper is to numerically study the spin-relaxation length in quantum wires.

In the presence of spin-orbit interaction, lack of inversion symmetry causes spin splitting in the absence of magnetic field. In two-dimensional (2D) systems, the asymmetry in the confining potential causes splitting linear in the wave vector.[3,4] This so-called Rashba term can be controlled by a gate voltage.[5,6] In a zinc-blende crystal, bulk inversion asymmetry causes the so-called Dresselhaus term,[7] cubic in the wave vector in bulk semiconductors, giving rise to linear and cubic terms in a heterostructure. It is known that the Rashba term is dominant over the Dresselhaus term in heterostructures consisting of narrow-gap semiconductors.

The existence of the Rashba spin splitting has a controversial history because the average field should vanish for a bound state, i.e., the gate electric field must be canceled by the field associated with the conduction-band offset at the interface.[8,9] In fact, the spin splitting is quite sensitive to boundary conditions at the surface in space-charge layers.[10–12] In quantum wells or heterostructures, the spin splitting can appear as a result of difference in band gaps and spin-orbit interactions between two materials.[13–28]

In the presence of the Rashba term, the electron spin precesses around the effective magnetic field perpendicular to the momentum. Controlling of this spin precession by the gate voltage is the key ingredient of the spin field effect transistor.[29] The spin Hall effect may be used for nonmagnetic spin-generation devices.[30–41] In such systems, even spin-independent impurity-scattering causes spin relaxation.

In this paper spin-relaxation length is calculated numerically in quantum wires, and its dependence on the wire width, the mean free path, and the strength of the spin-orbit interaction is elucidated. In Sec. II, the formulation to perform numerical calculations is presented. The subband structure and spin quantization are discussed in Sec. III. Some examples of the calculated results are given in Sec. IV and are discussed in Sec. V. A brief summary is given in Sec. VI. A method of actual numerical calculations is discussed in the Appendix.

II. FORMULATION

A. Quantum wires with spin-orbit interaction

The Hamiltonian of a two-dimensional system in the presence of spin-orbit interaction is given by

$$\mathcal{H} = \frac{\hbar^2 \boldsymbol{k}^2}{2m^*} + \alpha(k_x\sigma_y - k_y\sigma_x), \tag{1}$$

where m^* is the effective mass, $\boldsymbol{k}$ is the wave vector, and σ_x and σ_y are the Pauli spin matrices. The parameter α can be controlled by the gate electric field. This Hamiltonian shows that an effective Zeeman field for the spin depends on the electron momentum.

The eigenenergy of this Hamiltonian [Eq. (1)] is given by

$$\varepsilon_{\boldsymbol{k}s} = \frac{\hbar^2 \boldsymbol{k}^2}{2m^*} + s\alpha|\boldsymbol{k}|, \tag{2}$$

with spin index $s = \pm 1$. The strength of the spin-orbit interaction is characterized by the ratio of spin splitting at the Fermi level to the Fermi energy

$$\delta = \frac{\alpha k_F}{E_F}, \tag{3}$$

where k_F is the Fermi wave vector and E_F is the Fermi energy. For typical semiconductor 2D systems, the strength of the spin-orbit interaction is given by $\delta \lesssim 0.05$.

Let us consider a wire with width W. We shall take the x axis along the wire direction. In the absence of spin-orbit interaction, the subband energy is given by

$$\varepsilon_n(k) = \frac{\hbar^2}{2m^*}\left(\frac{n\pi}{W}\right)^2 + \frac{\hbar^2 k^2}{2m^*}, \quad (n = 1,2,\ldots), \tag{4}$$

where k is the wave vector in the wire direction. The channel number per spin of the wire, i.e., the number of occupied subbands below the Fermi level, is

$$N = \left[\frac{2W}{\lambda_F}\right], \tag{5}$$

where $[x]$ is an integer part of x. For sufficiently narrow wires, in which the subband separation is much larger than the spin splitting at the Fermi level, each subband can be regarded as having its own spin splitting proportional to αk. The subband energy is approximately given by

$$\varepsilon_{ns}(k) \approx \frac{\hbar^2}{2m^*}\left(\frac{n\pi}{W}\right)^2 + \frac{\hbar^2 k^2}{2m^*} + s\alpha k, \quad (n = 1,2,\ldots). \quad (6)$$

With the increase in the wire width, the subband structure exhibits complicated behavior depending on the spin splitting and the subband separation. In fact, the subband anticrossing starts to take place at the Fermi level when the spin splitting at the Fermi level $2\delta E_F$ exceeds the minimum subband spacing, $\varepsilon_2(k_F)-\varepsilon_1(k_F)=3\lambda_F^2 E_F/(4W^2)$. This condition can be written as $W>W_1$ with $W_1/\lambda_F=\sqrt{3/(8\delta)}$, showing that the anticrossing can play important roles in quantum wires.

When the spin splitting $2\alpha k_F$ at the Fermi level is close to the typical subband spacing $\sim E_F/N$, subbands with different spins become mixed with each other considerably, and the system looses the feature of the quantum wire and essentially turns into 2D. This condition is written as $W\sim W_2$ with $W_2/\lambda_F=1/(2\delta)$. For typical strength of the spin-orbit interaction, this corresponds to channel number $N\gtrsim 20$, for which the subband quantization has no strong influence on its electronic properties. Therefore, most quantum wires are in the regime $W\lesssim W_2$, showing that many of the subbands still have their own spin splitting and that the anticrossing can take place only for a few low-lying subbands.

B. Tight-binding model

In this study, a square-lattice tight-binding model with lattice constant a is used to simulate a quantum wire with spin splitting due to structure inversion asymmetry.[42] The Hamiltonian is given by

$$\mathcal{H} = -\sum_{\boldsymbol{n}} \sum_{\xi=\pm x,\pm y} c^\dagger_{\boldsymbol{n}+\boldsymbol{e}_\xi} T_\xi c_{\boldsymbol{n}} + 4t_1 \sum_{\boldsymbol{n}} c^\dagger_{\boldsymbol{n}} c_{\boldsymbol{n}}, \quad (7)$$

where T's are the hopping integrals between the nearest-neighbor atoms in each direction, given by

$$T_{\pm x} = \begin{pmatrix} t_1 & \pm t_2 \\ \mp t_2 & t_1 \end{pmatrix}, \quad T_{\pm y} = \begin{pmatrix} t_1 & \mp it_2 \\ \mp it_2 & t_1 \end{pmatrix}, \quad (8)$$

and $c^\dagger_{\boldsymbol{n}}$ and $c_{\boldsymbol{n}}$ are creation and annihilation operators at site $\boldsymbol{n}$, respectively. For this matrix representation, the spin basis has been chosen to be

$$|\uparrow\rangle = \begin{pmatrix} 1 \\ 0 \end{pmatrix}, \quad |\downarrow\rangle = \begin{pmatrix} 0 \\ 1 \end{pmatrix}. \quad (9)$$

In the momentum representation, this Hamiltonian can be written as

$$\mathcal{H}(\boldsymbol{k}) = 4t_1 - 2t_1[\cos(k_x a) + \cos(k_y a)] + 2t_2[\sin(k_x a)\sigma_y - \sin(k_y a)\sigma_x]. \quad (10)$$

In the continuum limit $|\boldsymbol{k}|a \ll 1$ this Hamiltonian is reduced to Eq. (1) with $m^*=\hbar^2/2t_1a^2$ and $\alpha=2t_2a$.

We shall measure almost all quantities in units of corresponding quantities in the continuum limit at the Fermi level instead of the tight-binding parameters. The diagonal hopping integral t_1 is given by

$$\frac{t_1}{E_F} = \left(\frac{\lambda_F}{2\pi a}\right)^2, \quad (11)$$

with the Fermi wavelength λ_F. The off-diagonal hopping integral is written as

$$\frac{t_2}{E_F} = \frac{\delta}{4\pi}\frac{\lambda_F}{a}. \quad (12)$$

It should be noted that because of the presence of small nonparabolicity present in the tight-binding model, i.e., slight deviation in the dispersion from Eq. (1), the channel number is slightly different from that given by Eq. (5) and that anticrossing starts to occur at W slightly different from $W_1/\lambda_F=\sqrt{3/(8\delta)}$.

The disorder effect is included by random on-site potential $u_{\boldsymbol{n}}$ which is uniformly distributed in the region $-U/2<u_{\boldsymbol{n}}<U/2$. The disorder strength is characterized by mean free path Λ in 2D, i.e.,

$$\frac{U}{E_F} = \sqrt{\frac{6\lambda_F^3}{\pi^3 a^2 \Lambda}}. \quad (13)$$

For $\Lambda>W$, the one-dimensional subbands are well defined, while they are completely destroyed for $\Lambda<W$. The former will be called the quantum-wire regime and the latter the dirty-wire regime.

We consider a system with M sites in width and N sites in length, described by Hamiltonian $\mathcal{H}$. An ideal lead consisting of an infinitely long wire with the same width without spin-orbit interaction, i.e., $t_2=0$, is connected to each end. We calculate the transmission coefficient through the system using a recursive Green's function technique.[43,44] In the present system, the transmission-coefficient matrix becomes spin dependent due to the spin-orbit interaction and is written as

$$t = (t_{i\mu,j\nu}), \quad (14)$$

where i and j represent channels of transmitted and incident waves, respectively, and μ and ν represent the spin direction ($\uparrow$ or $\downarrow$). More details on the actual method will be discussed in the Appendix. In a continuum limit, the length of the wire is given by $L=Na$ and the width is given by $W=(M+1)a$.

The ideal leads connected to the quantum wire should not have spin-orbit interaction for the calculation of spin-dependent transmission coefficients. There appears small probability of reflection at the boundary between the quantum wire and the ideal lead because of the discontinuous change in the value of t_2. This does not influence the spin-relaxation length defined by the exponential length dependence of the spin-correlation function.

C. Spin-relaxation length

In terms of the transmission coefficient t, the amplitude of the wave function of out-going channel i for an electron, in-coming from channel j with unit flux and spin in the $\pm y$ direction can be written as

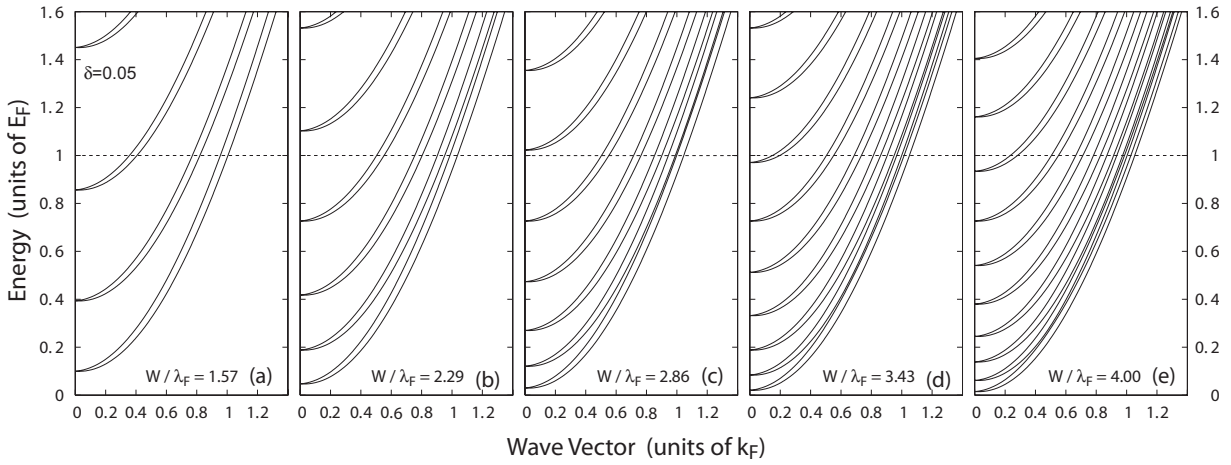

FIG. 1. Calculated subband dispersion relation for $\delta=0.05$ and $\lambda_F/a=7$. (a) $W/\lambda_F=1.57$, (b) 2.29, (c) 2.86, (d) 3.43, and (e) 4.00. The horizontal dashed line represents the Fermi level. Subband anticrossing starts to take place at the Fermi level when $W>W_1\approx 2.8\lambda_F$.

$$\psi_{i,j}^{\pm}(L)=\frac{1}{\sqrt{2}}\begin{pmatrix} t_{i\uparrow,j\uparrow} \\ t_{i\downarrow,j\uparrow} \end{pmatrix}+\frac{\pm i}{\sqrt{2}}\begin{pmatrix} t_{i\uparrow,j\downarrow} \\ t_{i\downarrow,j\downarrow} \end{pmatrix}. \tag{15}$$

Therefore, the average y spin of the transmitted wave is given by

$$\sigma_y^{\pm}(L)=\sum_{i,j}\psi_{i,j}^{\pm}(L)^{\dagger}\sigma_y\psi_{i,j}^{\pm}(L)\times\left(\sum_{i,j}|\psi_{i,j}^{\pm}(L)|^2\right)^{-1}. \tag{16}$$

This function can be understood as transmitted spin σ_y at $x=L$ for an electron incident at $x=0$ with spin $\sigma_y=\pm 1$. Then, the spin-correlation function for $\sigma_y(0)$ at $x=0$ and $\sigma_y(L)$ at $x=L$ may be defined as

$$\langle\sigma_y(0)\sigma_y(L)\rangle\propto F_{yy}(L)\equiv\frac{1}{2}\sum_{\pm}(\pm)\sigma_y^{\pm}(L). \tag{17}$$

As will be shown in the following, this function decays exponentially with L. Therefore, we define the spin-relaxation length Λ_S from the relation

$$\langle F_{yy}(L)\rangle\propto\exp\left(-\frac{L}{\Lambda_S}\right), \tag{18}$$

where $\langle\cdots\rangle$ means the sample average. Spin-correlation functions for other spin directions can be obtained by linear combination of $\sigma_y^{\pm}(L)$, but exhibit the same exponential decay with L for sufficiently large L.

In the following, we choose the strength of the spin splitting as $\delta=0.02$, 0.03, and 0.05. The Fermi wavelength is chosen to be $\lambda_F/a=7$, for which the continuum approximation is valid. Then, we have $W_1/\lambda_F\approx 4.5$ for $\delta=0.02$, $W_1/\lambda_F\approx 3.7$ for $\delta=0.03$, and $W_1/\lambda_F\approx 2.8$ for $\delta=0.05$. In an InGaAs/AlGaAs quantum well characterized by electron concentration $n_s=2\times 10^{12}$ cm^{-2} and effective mass $m^*/m_0=0.05$ with free-electron mass m_0, we have $\alpha=5.4\times 10^{-12}$ eV m for $\delta=0.02$, $\alpha=8.1\times 10^{-12}$ eV m for $\delta=0.03$, and $\alpha=1.4\times 10^{-11}$ eV m for $\delta=0.05$ with the Fermi energy of 95.8 meV and the Fermi wavelength of 17.7 nm. Systematic calculations are performed for $1\le W/\lambda_F\le 5.5$ and for $1\le\Lambda/\lambda_F\le 50$. In the InGaAs/AlGaAs quantum well, the corresponding width is $1.8\le W\le 9.7$ nm and the corresponding mobility is $7.6\times 10^3\le\mu\le 3.8\times 10^5$ cm^2/Vs. The sample average is performed over more than 2000 different disorder configurations.

III. SPIN SPLITTING IN QUANTUM WIRE

Figure 1 shows examples of the subband structure obtained in the tight-binding model for $\delta=0.05$. For a narrow wire with weak spin splitting as in Figs. 1(a) and 1(b), i.e., for $W<W_1$, subband anticrossing does not take place below the Fermi level. When W exceeds W_1 with the increase in the width, anticrossing of subbands with different spins occur starting with lower subbands. For largest $W/\lambda_F=4$, the spin splitting exceeds separations of several low-lying subbands.

The top panels of Fig. 2 show examples of calculated y-spin expectation value at the Fermi level as a function of W for (a) $\delta=0.02$, (b) 0.03, and (c) 0.05. Both x and z components of the spin expectation value identically vanish. For $W<W_1$, the y-spin expectation value is close to either +1 or −1, showing that the spin is well defined. When $W\sim W_1$, the $\sigma_y=+1$ branch of the lowest subband and −1 branch of the next-lowest subband cross each other at the Fermi level, and the spin expectation value is exchanged between the subbands. This occurs at every subband anticrossing. Due to the absence of anticrossing in the −1 branch of the lowest subband, it has $\sigma_y=-1$ with even increase in the width.

How well the spin is assigned to each subband may be measured by

$$S_y^2=\sum_j\langle\sigma_y\rangle_j^2 \tag{19}$$

or by S_y^2/N', where N' is the total number of subbands below the Fermi level including spin, j denotes subbands, and the spin expectation value $\langle\sigma_y\rangle_j$ should be taken at the Fermi level. The middle and bottom panels of Fig. 2 show S_y^2 and S_y^2/N', respectively. This average spin takes a dip at each anticrossing and gradually decreases with the increase in W.

IV. SPIN-RELAXATION LENGTH

Figure 3 shows calculated $\langle F_{yy}(L)\rangle$ for $\delta=0.05$ and $W/\lambda_F=3.86$. The spin-correlation function decays exponen-

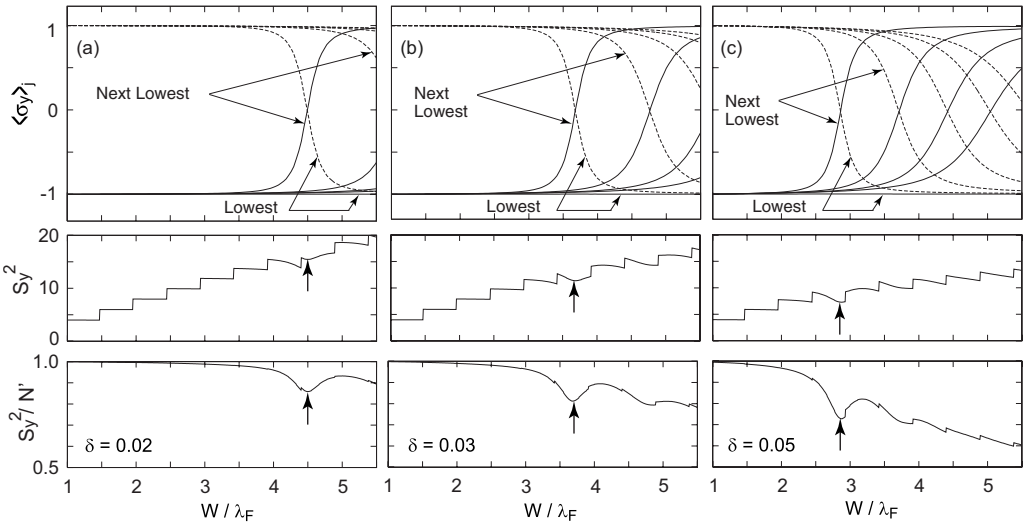

FIG. 2. Calculated y-spin expectation values of low-lying subbands as function of the width for (a) δ=0.02, (b) 0.03, and (c) 0.05. The top panels show $\langle\sigma_y\rangle_j$, the middle panels show S_y^2, and the bottom panels show S_y^2/N'. The arrows indicate the anticrossing of the spin-split lowest and first-excited subbands.

tially with the increase in the length for sufficiently large L, as we have mentioned before. By fitting the results to Eq. (18), we can determine the spin-relaxation length Λ_S.

Figure 4 shows resulting Λ_S as a function of W for (a) δ =0.02, (b) 0.03, and (c) 0.05. In the quantum-wire regime $\Lambda \gg W$, Λ_S becomes shorter when the Fermi energy is close to the subband edge. This is caused by strong scattering due to the singular density of states of one-dimensional subbands. With the increase in disorder or with the decrease in Λ, this variation within each channel number decreases and Λ_S decreases smoothly with W when $\Lambda < W$.

In the quantum-wire regime, in particular, Λ_S has a large dip structure near $W/\lambda_F \approx 4.5$ for δ=0.02 in Fig. 4(a), near $W/\lambda_F \approx 3.7$ for δ=0.03 in Fig. 4(b), and near $W/\lambda_F \approx 2.8$ for δ=0.05 in Fig. 4(c), as indicated by vertical arrows. These dips correspond well to those of S_y^2/N' shown in the middle and bottom panels of Fig. 2, i.e., $W \sim W_1$. For δ=0.05, in particular, the dip structure starts to disappear for Λ/λ_F=20 and becomes nearly absent for Λ/λ_F=5 within error bars. Therefore, the critical mean free path is larger than width W. This is to be expected because the anticrossing occurs between low-lying subbands, with an energy difference smaller than the mean subband spacing E_F/N. The critical mean free path is larger than W for δ=0.02 and 0.03, although it cannot clearly be determined.

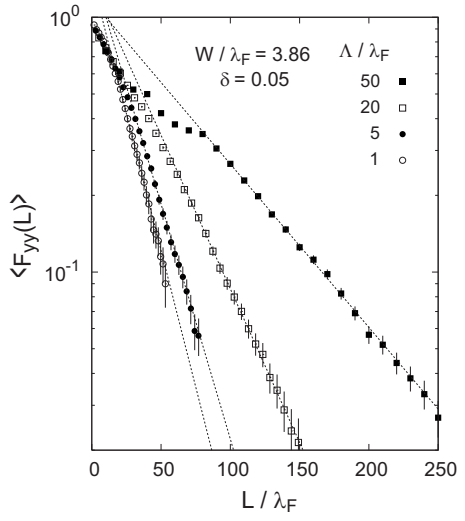

FIG. 3. Calculated spin-correlation function $\langle F_{yy}(L)\rangle$ for W/λ_F =3.86 and δ=0.05. The straight dotted lines show Eq. (18) for corresponding Λ_S.

There is a general tendency that Λ_S decreases with the increase in width W or channel number N. For largest Λ, in particular, the relaxation length at energies away from subband edges decreases with width W almost exponentially for W smaller than the anticrossing point W_1 denoted by the arrows, and the reduction with W becomes weaker after the anticrossing as more clearly seen for δ=0.05. With the decrease in Λ, the W dependence of Λ_S becomes similar for δ=0.02, 0.03, and 0.05 with absolute values roughly proportional to δ^{-2}. In the dirty limit Λ/λ_F=1, in particular, Λ_S exhibits a near-power-law dependence on W except in the region of small W. Figure 4 contains $\Lambda_S/\lambda_F \propto (W/\lambda_F)^{-3/2}$ for comparison. The exponent 3/2 is different from that expected in a 2D system with finite width as will be discussed in Sec. V.

Figure 5 shows Λ_S averaged over those of the same channel number as a function of mean free path Λ for (a) δ =0.02 and (b) 0.05. The error bars denote the range of the maximum and minimum values for each channel number. For the smallest channel number N=2 corresponding to $W/\lambda_F \approx 1$, Λ_S is proportional to Λ for all cases δ=0.02, 0.03 (not shown here), and 0.05. Although we have numerical data only for three different values of δ, it is safe to conclude that $\Lambda_S \propto \Lambda/\delta^2$ (actually, $\Lambda_S \sim 0.5 \times \Lambda/\delta^2$).

When the spin in each one-dimensional subband is purely in the $+y$ or $-y$ direction, the scattering processes conserving spin do not cause any spin relaxation. In actual narrow wires, however, the spin makes a slight precession around the y axis due to mixing between different subbands and the precession

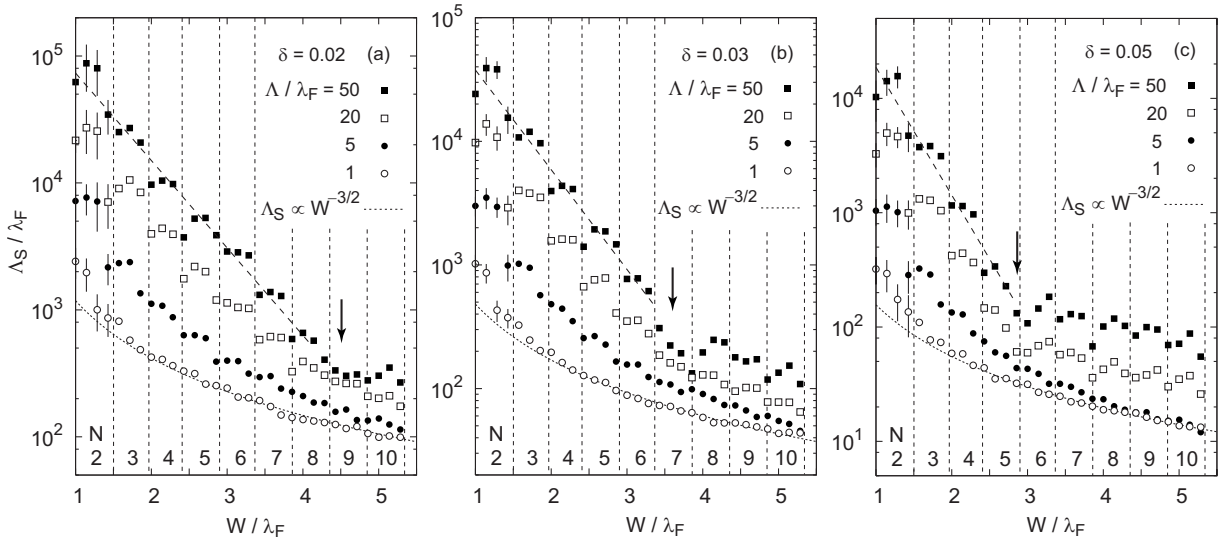

FIG. 4. Calculated spin-relaxation length Λ_S versus wire width W for (a) δ=0.02, (b) 0.03, and (c) 0.05. The values of mean free path Λ are listed together with corresponding symbols. The width where a large dip occurs in S_y^2/N' is denoted by the downward arrows. Typical error bars are shown only for the data with N=2. The vertical dashed lines represent the wire width corresponding to the Fermi-level crossing of a subband bottom and the numbers denote channel number N. The dotted curves show the power-law dependence $\Lambda_S \propto W^{-3/2}$ and the dashed straight lines show the exponential dependence.

frequency varies slightly between different subbands. This variation, giving rise to spin relaxation, is proportional to δ^2 because it appears in the second order with respect to the term $-\alpha k_y \sigma_x$ of the Hamiltonian.

In the case of very small channel number, the electron wave function is localized exponentially and the localization length is of the order of the mean free path Λ, i.e., the wave function decays exponentially like $\psi(L) \sim \exp(-L/\Lambda)$.[44–51] This means that the spatial dependence of the electron wave function is characterized by a single length scale of Λ. Therefore, the dependence $\Lambda_S \propto \Lambda/\delta^2$ obtained here is quite natural.

The spin-relaxation length for small N is more than two orders of magnitude larger than the mean free path and, therefore, larger than the localization length, showing that the spin is hardly relaxed even when the wave function becomes exponentially small. In the regime of strong localization, the localization length is known to depend on the way of averaging,[44,46] and the situation is likely to be the same for the spin-relaxation length. However, this does not affect the above conclusion that the spin relaxation does not practically take place for the transmitted electron wave in sufficiently narrow quantum wires.

With the increase in the channel number, the spin-relaxation length decreases and the suppression of the spin relaxation starts to take place for short Λ, i.e., the dependence of Λ_S on Λ becomes weaker and eventually vanishes. The figure shows that the suppression becomes appreciable when Λ becomes smaller than or comparable to W (the shaded region shows $\Lambda \sim W$). For Λ smaller than W, the one-dimensional subbands are destroyed by impurity scattering and the system becomes similar to a dirty 2D system, where the spin-relaxation length is known to be independent of the mean free path (see Sec. V).[52]

V. DISCUSSION

The Hamiltonian [Eq. (1)] in 2D shows that the spin performs precession around an effective magnetic field perpendicular to the momentum. Although the spin is conserved by impurity scattering, the spin precesses around a different direction after each scattering event and spin relaxation takes place. The important parameter is a typical spin precession angle $\omega\tau$ between successive collisions, where $\omega = 2\alpha k_F/\hbar$ is the spin precession frequency at the Fermi level and τ is the momentum relaxation time.[52] We have $\omega\tau = 2\alpha k_F(\hbar/\tau)^{-1} = 2\pi\delta(\Lambda/\lambda_F)$.

In the clean limit $\omega\tau \gg 1$, the spin precesses many times before each scattering and the spin-relaxation length is proportional to the mean free path, i.e., $\Lambda_S \propto \Lambda$. In the dirty regime $\omega\tau \ll 1$, the precession angle between successive scatterings remains small. In 2D the spin diffuses on Bloch's sphere with diffusion constant $D_S = (\omega\tau)^2/(2\tau)$ and the spin-relaxation time τ_S is determined through $D_S\tau_S = 1$ as $\tau_S = 2/(\omega^2\tau)$.[52] This is closely related to motional narrowing effects.[53–55] The spin-relaxation length, defined as $\Lambda_S = \sqrt{D\tau_S}$ with diffusion constant $D = \Lambda^2/(2\tau)$, becomes $\Lambda_S = v_F/\omega$ independent of Λ.

When an electron is confined into a wire, a part of the spin precession corresponding to the motion perpendicular to the wire approximately cancels out due to reflection at the wall, leading to suppression of the spin relaxation. This effect was previously studied in the regime $\omega\tau \ll 1$ and $W \gg \Lambda$. In fact, a classical Monte Carlo simulation[56] showed that the suppression occurs when the width becomes smaller than the spin-relaxation length v_F/ω in 2D and gave the spin-relaxation length $\Lambda_S \propto (v_F/\omega)^2 W^{-1}$. A similar result was obtained by other methods such as a spin-diffusion equation.[57,58] The relaxation length in the regime $W < \Lambda$ was

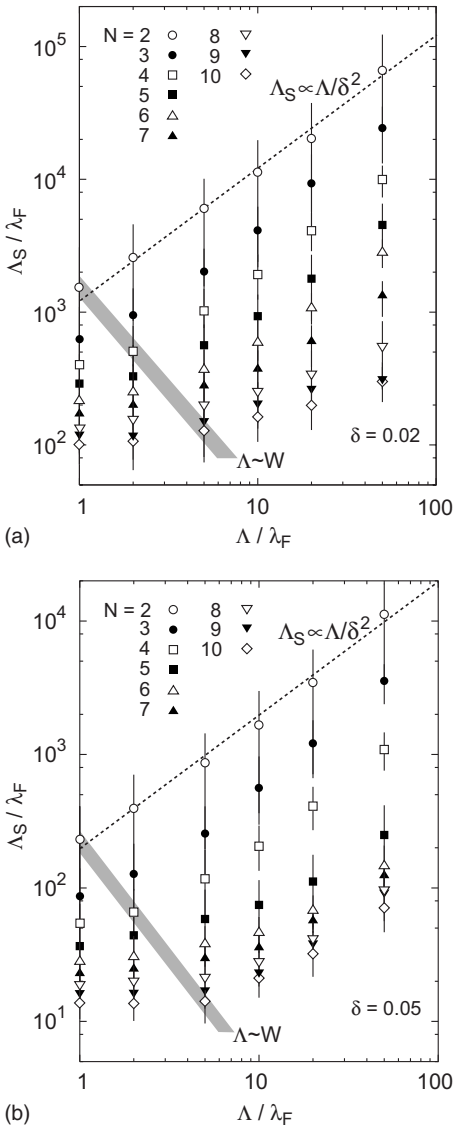

FIG. 5. Λ_S averaged over the same channel number as a function of Λ for (a) δ=0.02 and (b) 0.05. The dotted lines show $\Lambda_S = 0.5 \times \Lambda/\delta^2$ and the shaded regions correspond to $\Lambda \sim W$.

suggested to be enhanced and multiplied by $\sqrt{\Lambda/W}$,[58] i.e., $\Lambda_S \propto (v_F/\omega)^2 \Lambda^{1/2} W^{-3/2}$, based on an analogy to the so-called flux cancellation effect.[59] Suppression of spin relaxation has experimentally been observed using Faraday rotation in InGaAs submicron wire.[60,61]

In the numerical results, Λ_S becomes independent of Λ and increases with the decrease in W in dirty wires $W \lesssim \Lambda$. This is qualitatively in agreement with the behavior of 2D systems with finite width. Quantitatively, however, we have $\Lambda_S \propto W^{-\eta}$ with $\eta \sim 1.5$ for $\Lambda/\lambda_F = 1$, different from W^{-1} and rather coincident with the 2D result in the different regime $W < \Lambda$. As has already been discussed, the spin relaxation in quantum wires is sensitive to the relative magnitude of the spin splitting and the subband separation and to the associated anticrossing. The present results show, therefore, that the importance of the nature of the spin-split subbands prevails even in the dirty limit where the one-dimensional subbands have mostly been destroyed.

When an electron can move only along a straight line, the spin precession during the electron motion in one direction is exactly canceled by that in the opposite direction, and therefore, no spin relaxation occurs by spin-conserving scattering. The present numerical calculations have demonstrated that this strong suppression of the spin relaxation is effective as long as the quantum confinement gives severe restriction to the electron motion perpendicular to the quantum wire and the spin splitting is smaller than the corresponding subband separations.

The spin relaxation exhibits a near singular dependence on the Fermi level in a narrow quantum wire with only a single channel. In the vicinity of the bottom of the second subband, Λ_S remains of the same order as that for $N=2$ presumably due to strong subband mixing. With the decrease in the Fermi level, this mixing diminishes and then the spin-relaxation length becomes extremely long and quickly exceeds the length accessible by numerical calculations. This shows that in a practical sense the spin relaxation is perfectly suppressed and Λ_S becomes infinite in a narrow wire in the quantum limit. Understanding details of the Fermi-level dependence requires more elaborate numerical calculations and is beyond the scope of the present study.

It should be noted that the time and spatial evolutions of spin can be quite different in quantum wires. In fact, in the quantum limit with only a single channel, the spin-relaxation time becomes finite because the spin direction becomes at random after a sufficiently long time. However, the spin-relaxation length is quite long because the spin at a given position is always the same for an electron moving in the same direction. Therefore, the spin-relaxation length Λ_S and relaxation time τ_S can be quite different in quantum wires.

So far, we have completely neglected terms due to bulk inversion asymmetry. If the strength of the linear Dresselhaus term is comparable to the Rashba term, a strong anisotropy appears in the spin splitting and also in the spin relaxation. This anisotropic spin relaxation is expected to be suppressed with the decrease in the wire width. In this case, however, cubic Dresselhaus terms can become important in the spin relaxation.[57,58] Furthermore, even if effects due to the bulk inversion asymmetry are sufficiently weak, the so-called Elliott-Yafet mechanism[62,63] eventually takes over the spin relaxation in narrow quantum wires.

VI. SUMMARY

The spin-relaxation length in quantum wires with the spin splitting due to the lack of the structure inversion symmetry has been numerically studied using a tight-binding model. In this system spin-independent impurity causes spin relaxation. It has been shown that the spin-relaxation length is sensitive to the spin-split subband structure in quantum wires, in particular to the relative magnitude of the spin splitting and the subband separations. When the spin splitting is sufficiently smaller than the subband separations, the quantized one-dimensional subbands have a well-defined spin, and the spin-relaxation length is considerably enhanced with the decrease in the width.

ACKNOWLEDGMENTS

This work was supported in part by a 21st Century COE Program at Tokyo Tech "Nanometer-Scale Quantum Physics" from the Ministry of Education, Culture, Sports, Science and Technology, Japan.

APPENDIX: RECURSIVE CALCULATION

The transmission coefficient t of the square-lattice system with M sites in width and N sites in length can be calculated using the Green's function G_{N1} given by an (M,M) matrix, connecting the left boundary with $n_x=1$ and the right boundary with $n_x=N$. An explicit formula for t in terms of G_{N1} is essentially the same as that given previously[43,44] except that in the ideal leads the spin-orbit interaction is absent, and therefore, the spin is decoupled from the orbital motion. This makes the actual calculation of t from G_{N1} much simpler because both wave functions and energies of the channels in the lead are analytically obtained. The Green's function G_{N1} can be calculated by a recursive method, starting with G_{11}, then G_{21} and G_{31}, and so on. However, this calculation should be performed with special care as will be discussed below.

In the presence of spin-orbit interaction, the matrix elements of the Hamiltonian and the Green's function in spin space is given by a quaternion real, written as

$$a=\sum_{j=0}^{3} a_j\tau_j=\begin{pmatrix} a_0+ia_1 & a_2+ia_3 \\ -a_2+ia_3 & a_0-ia_1 \end{pmatrix}, \tag{A1}$$

with real a_j and

$$\tau_0=\begin{pmatrix} 1 & 0 \\ 0 & 1 \end{pmatrix},\quad \tau_1=\begin{pmatrix} i & 0 \\ 0 & -i \end{pmatrix},\quad \tau_2=\begin{pmatrix} 0 & 1 \\ -1 & 0 \end{pmatrix},\quad \tau_3=\begin{pmatrix} 0 & i \\ i & 0 \end{pmatrix}. \tag{A2}$$

When we calculate the Green's functions recursively using complex matrices instead of quaternion real matrices, elements not given by a quaternion real will appear by numerical errors and may grow after many iterations, destroying the symmetry of the system.[42] In Ref. 42 direct quaternion algebra was used for the recursive calculation of the Green's functions. Similar methods were used by other calculations.[64–67] In this study, we use complex matrices but make frequent corrections to keep the symmetry in order to avoid this numerical instability.

Let us consider a wire consisting of $N+2$ sites in length from 0 to $N+1$. For the calculation of the transmission coefficient, we have to attach an ideal lead to sites 0 and $N+1$. The effect of attached ideal leads is included as a complex self-energy term at site 0 and $N+1$.[43] As a result, the effective Hamiltonians for these sites are not given by quaternion real numbers. The symmetry is perfectly kept when we connect sites 0 and $N+1$ after the calculation of the necessary Green's functions for sites 1 and N. The connection of sites 0 and $N+1$ attached to an ideal lead can be made in a straightforward manner when we have the appropriate Green's functions for sites 1 and N.

A numerical instability may occur in the recursive calculation of the Green's functions for sites 1 and N for large N, but can be removed as follows: Let G be an element of the Green's function in the spin space,

$$G=\begin{pmatrix} A & B \\ C & D \end{pmatrix}, \tag{A3}$$

with complex number A, B, C, and D. For quaternion real G, $\mathrm{Im}(A+D)$, $\mathrm{Re}(A-D)$, $\mathrm{Im}(B-C)$, and $\mathrm{Re}(B+C)$ should identically vanish, but become nonzero after many iterations due to round-off errors. Therefore, after each iteration, we replace G with a quaternion real G_{corr}, given by

$$G_{\mathrm{corr}}=\frac{1}{2}\mathrm{Re}(A+D)\tau_0+\frac{1}{2}\mathrm{Im}(A-D)\tau_1+\frac{1}{2}\mathrm{Re}(B-C)\tau_2+\frac{1}{2}\mathrm{Im}(B+C)\tau_3. \tag{A4}$$

In this way, we can successfully avoid the numerical instability.

[1] *Semiconductor Spintronics and Quantum Computation*, edited by D. D. Awschalom, D. Loss, and N. Samarth (Springer, Berlin, 2002).
[2] I. Zutic, J. Fabian, and S. Das Sarma, Rev. Mod. Phys. **76**, 323 (2004).
[3] F. J. Ohkawa and Y. Uemura, J. Phys. Soc. Jpn. **37**, 1325 (1974).
[4] Yu. A. Bychkov and E. I. Rashba, J. Phys. C **17**, 6039 (1984).
[5] J. Nitta, T. Akazaki, H. Takayanagi, and T. Enoki, Phys. Rev. Lett. **78**, 1335 (1997).
[6] G. Engels, J. Lange, Th. Schäpers, and H. Lüth, Phys. Rev. B **55**, R1958 (1997).
[7] G. Dresselhaus, Phys. Rev. **100**, 580 (1955).
[8] A. Darr, J. P. Kotthaus, and T. Ando, *Proceedings of the 13th International Conference on Physics of Semiconductors* (Tipographia Marves, Rome, 1976), p. 774.
[9] T. Ando, A. B. Fowler, and F. Stern, Rev. Mod. Phys. **54**, 437 (1982), and references cited therein.
[10] Y. Takada, K. Arai, N. Uchimura, and Y. Uemura, J. Phys. Soc. Jpn. **49**, 1851 (1980).
[11] G. E. Marques and L. J. Sham, Surf. Sci. **113**, 131 (1982).
[12] T. Ando, J. Phys. Soc. Jpn. **54**, 2676 (1985).
[13] R. Lassnig, Phys. Rev. B **31**, 8076 (1985).
[14] G. Lommer, F. Malcher, and U. Rössler, Phys. Rev. Lett. **60**, 728 (1988).
[15] L. Wissinger, U. Rossler, R. Winkler, B. Jusserand, and D. Richards, Phys. Rev. B **58**, 15375 (1998).
[16] R. Winkler, Phys. Rev. B **62**, 4245 (2000).
[17] R. Winkler, Physica E **22**, 450 (2004).
[18] R. Winkler, Phys. Rev. B **69**, 045317 (2004).
[19] P. Pfeffer and W. Zawadzki, Phys. Rev. B **52**, R14332 (1995).

[20] P. Pfeffer, Phys. Rev. B **55**, R7359 (1997).
[21] P. Pfeffer, Phys. Rev. B **59**, 15902 (1999).
[22] P. Pfeffer and W. Zawadzki, Phys. Rev. B **59**, R5312 (1999).
[23] W. Zawadzki and P. Pfeffer, Phys. Rev. B **64**, 235313 (2001).
[24] P. Pfeffer and W. Zawadzki, Phys. Rev. B **68**, 035315 (2003).
[25] B. Das, S. Datta, and R. Reifenberger, Phys. Rev. B **41**, 8278 (1990).
[26] W. Knap, C. Skierbiszewski, A. Zduniak, E. Litwin-Staszewska, D. Bertho, F. Kobbi, J. L. Robert, G. E. Pikus, F. G. Pikus, S. V. Iordanskii, V. Mosser, K. Zekentes, and Yu. B. Lyanda-Geller, Phys. Rev. B **53**, 3912 (1996).
[27] J. P. Heida, B. J. van Wees, J. J. Kuipers, T. M. Klapwijk, and G. Borghs, Phys. Rev. B **57**, 11911 (1998).
[28] Th. Schäpers, G. Engels, J. Lange, Th. Klocke, M. Hollfelder, and H. Lüth, J. Appl. Phys. **83**, 4324 (1998).
[29] S. Datta and B. Das, Appl. Phys. Lett. **56**, 665 (1990).
[30] J. Sinova, D. Culcer, Q. Niu, N. A. Sinitsyn, T. Jungwirth, and A. H. MacDonald, Phys. Rev. Lett. **92**, 126603 (2004).
[31] J. Inoue, G. E. W. Bauer, and L. W. Molenkamp, Phys. Rev. B **70**, 041303(R) (2004).
[32] E. I. Rashba, Phys. Rev. B **70**, 201309(R) (2004).
[33] E. G. Mishchenko, A. V. Shytov, and B. I. Halperin, Phys. Rev. Lett. **93**, 226602 (2004).
[34] O. Chalaev and D. Loss, Phys. Rev. B **71**, 245318 (2005).
[35] R. Raimondi and P. Schwab, Phys. Rev. B **71**, 033311 (2005).
[36] O. V. Dimitrova, Phys. Rev. B **71**, 245327 (2005).
[37] K. Nomura, J. Sinova, N. A. Sinitsyn, and A. H. MacDonald, Phys. Rev. B **72**, 165316 (2005).
[38] V. V. Bryksin and P. Kleinert, Phys. Rev. B **73**, 165313 (2006).
[39] A. Khaetskii, Phys. Rev. Lett. **96**, 056602 (2006).
[40] A. V. Shytov, E. G. Mishchenko, H. A. Engel, and B. I. Halperin, Phys. Rev. B **73**, 075316 (2006).
[41] K. Arii, M. Koshino, and T. Ando, Phys. Rev. B **76**, 045311 (2007).
[42] T. Ando, Phys. Rev. B **40**, 5325 (1989).
[43] T. Ando, Phys. Rev. B **44**, 8017 (1991).
[44] T. Ando and H. Tamura, Phys. Rev. B **46**, 2332 (1992).
[45] A. A. Abrikosov and I. A. Ryzhkin, Adv. Phys. **27**, 147 (1978).
[46] P. W. Anderson, D. J. Thouless, E. Abrahams, and D. S. Fisher, Phys. Rev. B **22**, 3519 (1980).
[47] P. W. Anderson, Phys. Rev. B **23**, 4828 (1981).
[48] O. N. Dorokhov, Zh. Eksp. Teor. Fiz. **85**, 1040 (1983) [Sov. Phys. JETP **58**, 606 (1983)].
[49] K. B. Efetov and A. I. Larkin, Zh. Eksp. Teor. Fiz. **85**, 764 (1983) [Sov. Phys. JETP **58**, 444 (1983)].
[50] A. A. Abrikosov, Phys. Scr. **T27**, 148 (1989).
[51] J.-L. Pichard, M. Sanquer, K. Slevin, and P. Debray, Phys. Rev. Lett. **65**, 1812 (1990).
[52] M. I. D'yakonov and V. I. Perel', Zh. Eksp. Teor. Fiz. **60**, 1954 (1971) [Sov. Phys. JETP **33**, 1053 (1971)].
[53] P. W. Anderson and P. R. Weiss, Rev. Mod. Phys. **25**, 269 (1953).
[54] R. Kubo and K. Tomita, J. Phys. Soc. Jpn. **9**, 888 (1954).
[55] R. Kubo, J. Phys. Soc. Jpn. **9**, 935 (1954).
[56] A. A. Kiselev and K. W. Kim, Phys. Rev. B **61**, 13115 (2000).
[57] A. G. Mal'shukov and K. A. Chao, Phys. Rev. B **61**, R2413 (2000).
[58] S. Kettemann, Phys. Rev. Lett. **98**, 176808 (2007).
[59] C. W. J. Beenakker and H. van Houten, Phys. Rev. B **37**, 6544 (1988).
[60] A. W. Holleitner, V. Sih, R. C. Myers, A. C. Gossard, and D. D. Awschalom, Phys. Rev. Lett. **97**, 036805 (2006).
[61] A. W. Holleitner, V. Sih, R. C. Myers, A. C. Gossard, and D. D. Awschalom, New J. Phys. **9**, 342 (2007).
[62] R. J. Elliott, Phys. Rev. **96**, 266 (1954).
[63] Y. Yafet, in *Solid State Physics*, edited by F. Seitz and D. Turnbull (Academic, New York, 1963), Vol. 14, p. 1.
[64] T. Kawarabayashi, T. Ohtsuki, K. Slevin, and Y. Ono, Phys. Rev. Lett. **77**, 3593 (1996).
[65] Y. Asada, K. Slevin, and T. Ohtsuki, Phys. Rev. Lett. **89**, 256601 (2002).
[66] Y. Asada, K. Slevin, and T. Ohtsuki, Phys. Rev. B **70**, 035115 (2004).
[67] Y. Asada, K. Slevin, and T. Ohtsuki, Phys. Rev. B **73**, 041102(R) (2006).